Coupled Systems Mechanics, *Vol. 13, No. 6 (2024) 471-483*
https://doi.org/10.12989/csm.2024.13.6.471

Isogeometric analysis of static bending steel UHPC composite slabs based on a refined plate theory

Van Minh Ngo*[1], Xuan Tung Nguyen[1a], Duy Hien Ta[1b] and Adnan Ibrahimbegovic[2c]

[1]University of Transport and Communications,
03 Cau Giay street, Lang Thang ward, Dong Da district, Hanoi, Vietnam
[2]Technical University of Compiegne, 60200 Compiègne, France

(Received July 18, 2024, Revised October 28, 2024, Accepted October 29, 2024)

Abstract. Ultra-High Strength Concrete (UHPC) has been widely used in construction with many advantages such as high compressive and tensile strength, high durability, and waterproofing. This paper developed an Isogeometric analysis (IGA) for static steel UHPC composite slab analysis. High-order shear strains using refined plate theory are considered when constructing equations describing plate behavior using the Isogeometric method. Various numerical examples have been performed and compared with analytical methods from previous studies as well as with the finite element method, showing the high accuracy of the proposed method in this study. The influence of plate parameters, such as the thickness of steel and concrete layers, on displacement, was investigated in detail.

Keywords: IGA; refined plate theory; steel UHPC composite slabs; UHPC

1. Introduction

Steel-concrete composite structures have been widely used in bridge structures (Thang and Anh 2021, El-Helou and Graybeal 2022, Shuwen *et al.* 2020, Xiao *et al.* 2022, Hien *et al.* 2022, Gunes *et al.* 2012), both highway and railway bridges, due to the advantages of the combination of the two materials, the reduction of height/span ratio, the reduction of deflection, and higher rigidity than a normal steel structure. For simple composite beams or plates, the compressive concrete on the top and tensile steel on the bottom will have high capacity of strength on the gravity load direction. However, for continuous beams or slabs with negative moment zones, the concrete works in tension and the lower flanges steel beam works in compressive condition, this often has limitations in terms of strength, load carrying capacity and service life of the structure.

Recently, UHPC has been used to solve the cracks of concrete decks and improve the load carrying capacity of deck slabs such as the Thang Long (Vietnam) bridge improvement bridge desk project (Nhiem 2020). Due to the favorable mechanical properties of UHPC materials, UHPC

*Corresponding author, Associate Professor, E-mail: minhngovan83@utc.edu.vn
[a]Associate Professor, E-mail: ngxuantung@utc.edu.vn
[b]Associate Professor, E-mail: tdhien@utc.edu.vn
[c]Professor, E-mail: adnan.ibrahimbegovic@utc.fr

http://www.techno-press.org/?journal=csm&subpage=8 ISSN: 2234-2184 (Print), 2234-2192 (Online)

slabs has thinner thicknesses to achieve the same capacity as conventional concrete slabs under the same loading conditions.

Recently, there have been many experimental and theoretical studies related to UHPC (Ibrahim *et al.* 2017, Wu *et al.* 2018, Micelli *et al.* 2020, Haruna *et al.* 2023, Wu *et al.* 2018, Liao *et al.* 2022). Antony Kodsy and George Morcous (Kodsy and Morcous 2022) predicted the Shear Strength of Ultra-High-Performance Concrete Beams without Transverse Reinforcement. Mohamed Abokifa and Mohamed Moustafa (Abokifa and Moustafa 2021) have experimentally studied the Precast Bridge Deck Systems with Non-Proprietary UHPC Transverse Field Joints. Deng *et al.* (2020) employed the experimental test of the lightweight steel-ultra-high-performance concrete composite bridge to study the behavior of joints in beams. Luu and Kim (2023) used Abaqus software to study the bond between the normal Concrete and Ultra High Performance Fiber-Reinforced Concrete. Zhu *et al.* (2022) studied shear behavior between waffle slabs and steel beams using experimental tests and the finite element method. El-Helou and Graybeal (2022) tested six bulb-tee UHPC pretensioned bridge girder specimens to investigate the shear strength of the beam. Cuong and Quang (2020) studied a test on the flexural behavior of prestressed textile-reinforced concrete plates. Liem *et al.* (2023) investigated the size impact on the fracture characteristics of ultrahigh-performance fiber-reinforced concrete. Ye *et al.* (2021) improve the mechanical performance of ultra-high-performance concrete (UHPC) composite plates by an experimental approach.

There are few theoretical studies on beam or slab calculation related to UHPC materials. The analytical and numerical methods have been studied and applied to plate structures. Ta and Noh (2015) approximated the displacement fields by the Navier approach to find the vibrational response of the functionally graded plates. Phuc (2020) developed a finite element method using phase field and third-order shear deformation theory to study the free vibration of cracked plates with varying thicknesses. Pham *et al.* (2023) developed a finite element method by combining the edge-based smoothed finite element method and tensorial components triangular element for dynamics of sandwich plates. Pu *et al.* (2022) studied the projectile penetration of steel plate reinforced concrete (SC) walls using finite element software LS-DYNA. Deepak and Preeti applied the finite element method to analyze the behavior of steel-concrete-steel sandwich plates. Akinropo and Morgan (2019) experiment with steel plate-strengthened reinforced concrete slabs under dynamic loading to investigate dynamic behavior. Hughes *et al.* (2005) studied the failure of Steel-Concrete-Steel Sandwich Slabs with Bi-Directional Corrugated-Strip Connectors by quasi-static loading test.

In complex structural problems, numerical methods have more advantages than analytical methods. The common numerical method is the finite element method, which has been developed for a long time for many types of structures, such as beams and shells. Recently, Thomas huge (Hughes *et al.* 2005, Cottrell *et al.* 2009) has proposed isogeometric analysis method with the ability to integrate geometric simulation and structure analysis, with higher accuracy. M. Lezgy-Nazargah developed isogeometric analysis for composite steel-concrete beams based on refined high-order shear deformation. Jun *et al.* (2019) proposed new 2D damage-plasticity model based on isogeometric analysis for the analysis nonlinear behavior of concrete. Tran *et al.* (2013) developed the isogeometric analysis for functionally graded plates considering the effect of higher-order shear deformation. Le-Manh *et al.* (2016) constructed the formulation of isogeometric analysis for composite plates considering the Green strains with small rotations. Zhang *et al.* (2023) developed a combination of isogeometric analysis and meshfree methods for static and dynamic crack propagation problems. Besides deterministic problems, some random problems have been studied on the basis of isogeometric analysis method. (Hien and Noh 2017, Ta and Nguyen 2020) researched and developed stochastic isogeometric analysis method for functionally graded material.

Although there have been many studies on slab using the isogeometric analysis method, none on steel UHPC composite slabs. This study will develop the isogeometric analysis method for steel UHPC composite slab considering the high-order shear strain

2. The NURBS functions

The B-spline basis functions and non-uniform rational B-spline (NURBS) functions (Piegl and Tiller 1997. Cottrell *et al.* 2009) create the isogeometric analysis method. To construct a set of n B-spline basis functions of order p, a knot vector Ξ is defined as a set of coordinates in the parametric space in one dimensional parametric domain of $\xi \in [0,1]$.

$$\Xi = \{\xi_1, \xi_2, \cdots, \xi_{n+p+1}\}, \quad \xi_i \le \xi_{i+1}$$
$$i = 1,2,\cdots,n+p \tag{1}$$

where ξ is the i-th knot, i is the knot index, p is the polynomial order.

Given the knot vector, the B-spline basis functions are defined recursively starting with piecewise constants (p=0) as follows

$$N_{i,0}(\xi) = \begin{cases} 1 & \text{if } \xi_i \leqslant \xi < \xi_{i+1}, \\ 0 & \text{otherwise.} \end{cases} \tag{2}$$

For p=1,2,3, …, they are defined by the following equation

$$N_{i,p}(\xi) = \frac{\xi-\xi_i}{\xi_{i+p}-\xi_i} N_{i,p-1}(\xi) + \frac{\xi_{i+p+1}-\xi}{\xi_{i+p+1}-\xi_{i+1}} N_{i+1,p-1}(\xi) \tag{3}$$

B-spline curves are constructed using a linear combination of B-spline basis functions with a coefficient vector. The elements of the coefficient vector of the basic functions are referred to as control points. Given n number of the p-th degree B-spline basis functions, $N_{i,p}$, i=1, 2, …, n, and corresponding control points B_i, i=1, 2, …, n, a piecewise-polynomial B-spline curve is given as

$$C(\xi) = \sum_{i=1}^{n} N_{i,p}(\xi) B_i \tag{4}$$

The tensor product of basic functions defines the B-spline surfaces in two parametric dimensions of ξ and η with two-knot vectors $\Xi = \{\xi_1, \xi_2, \dots, \xi_{n+p+1}\}$ and $\Phi = \{\eta_1, \eta_2, \dots, \eta_{m+q+1}\}$, and are expressed as follows

$$\boldsymbol{S}(\xi,\eta) = \sum_{i=1}^{n} \sum_{j=1}^{m} N_{i,p}(\xi) M_{j,q}(\eta) \boldsymbol{P}_{i,j} \tag{5}$$

where $N_{i,p}(\xi)$ and $M_{j,q}(\eta)$ are the B-spline basis functions defined on the knot vectors over an m×n net of control points.

Eq. (5) can be written in a simplified form as follows

$$\boldsymbol{S}(\xi,\eta) = \sum_{I=1}^{m\times n} N_I^b(\xi,\eta) \boldsymbol{P}_I \tag{6}$$

where $N_I^b(\xi,\eta) = N_{i,p}(\xi) M_{j,q}(\eta)$ is the shape function associated with control point I.

Adding individual weight w_I at each control point into the B-spline basis functions to construct

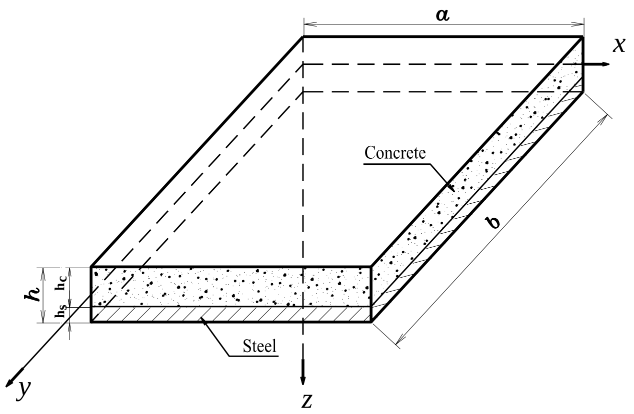

Fig. 1 Geometry of UHPC slabs

the non-uniform rational B-splines (NURBS) functions

$$R_{i,p}(\xi) = \frac{N_{i,p}(\xi)w_i}{\sum_{I=1}^{n} N_{I,p}^{b}(\xi)w_I} \tag{7}$$

where w_i are a set of n positive weights.

Generally, the NURBS surface of order p in ξ direction and order q in η direction can be expressed as

$$\boldsymbol{S}(\xi,\eta) = \sum_{I=1}^{m\times n} R_I(\xi,\eta)B_I \quad with\ R_I(\xi,\eta) = \frac{N_I^b w_I}{\sum_{I=1}^{m\times n} N_I^b(\xi,\eta)w_I} \tag{8}$$

3. Isogeometric formulations for steel UHPC composite slabs based on refined plate theory

Consider a rectangular slab of length a, width b, and thickness h made of functionally grade material, as shown in Fig. 1.

The displacements U,V,W of material point at (x,y,z) in the steel UHPC composite plates which take into account the shear deformation effect following the refined plate theory (Shimpi and Patel 2006) can be expressed as follows:

$$\begin{gathered} U = u_0 - z\frac{\partial w_b}{\partial x} + \left[\frac{1}{4}z - \frac{5}{3}z\left(\frac{z}{h}\right)^2\right]\frac{\partial w_s}{\partial x} \\ V = v_0 - z\frac{\partial w_b}{\partial y} + \left[\frac{1}{4}z - \frac{5}{3}z\left(\frac{z}{h}\right)^2\right]\frac{\partial w_s}{\partial y} \\ W = w_b + w_s \end{gathered} \tag{9}$$

where u_0, v_0, w_b, w_s are the displacement components on the mid-plane, respectively.

The linear strains can be obtained by differentiating equation as

$$\boldsymbol{\varepsilon} = \boldsymbol{\varepsilon}_0 + z\boldsymbol{\kappa}_b + \Psi\boldsymbol{\kappa}_s, \gamma = \chi\boldsymbol{\varepsilon}_s \tag{10}$$

where

$$\boldsymbol{\varepsilon} \quad = \begin{Bmatrix} \varepsilon_x \\ \varepsilon_y \\ \gamma_{xy} \end{Bmatrix}, \boldsymbol{\varepsilon}_0 = \begin{Bmatrix} \dfrac{\partial u_0}{\partial x} \\ \dfrac{\partial v_0}{\partial y} \\ \dfrac{\partial u_0}{\partial y} + \dfrac{\partial v_0}{\partial x} \end{Bmatrix}, \boldsymbol{\kappa}_b = \begin{Bmatrix} -\dfrac{\partial^2 w_b}{\partial x^2} \\ -\dfrac{\partial^2 w_b}{\partial y^2} \\ -2\dfrac{\partial^2 w_b}{\partial x \partial y} \end{Bmatrix},$$

$$\boldsymbol{\kappa}_s = \begin{Bmatrix} -\frac{\partial^2 w_s}{\partial x^2} \\ -\frac{\partial^2 w_s}{\partial y^2} \\ -2\frac{\partial^2 w_s}{\partial x \partial y} \end{Bmatrix}, \gamma = \begin{Bmatrix} \gamma_{yz} \\ \gamma_{xz} \end{Bmatrix}, \boldsymbol{\varepsilon}_s = \begin{Bmatrix} \frac{\partial w_s}{\partial y} \\ \frac{\partial w_s}{\partial x} \end{Bmatrix} \tag{11}$$

and

$$\Psi(z) = -\frac{1}{4}z + \frac{5}{3}z\left(\frac{z}{h}\right)^2 \ , \chi(z) = 5\left[\frac{1}{4} - \left(\frac{z}{h}\right)^2\ \right] \tag{12}$$

The linear constitutive relations of plates can be written for steel and concrete

$$for \quad steel \quad \begin{Bmatrix} \sigma_x \\ \sigma_y \\ \sigma_{yz} \\ \sigma_{xz} \\ \sigma_{xy} \end{Bmatrix} = \begin{bmatrix} Q_{11}^s & Q_{12}^s & 0 & 0 & 0 \\ Q_{12}^s & Q_{22}^s & 0 & 0 & 0 \\ 0 & 0 & Q_{44}^s & 0 & 0 \\ 0 & 0 & 0 & Q_{55}^s & 0 \\ 0 & 0 & 0 & 0 & Q_{66}^s \end{bmatrix} \begin{Bmatrix} \varepsilon_x \\ \varepsilon_y \\ \gamma_{yz} \\ \gamma_{xz} \\ \gamma_{xy} \end{Bmatrix} \tag{13}$$

$$for \quad concrete \quad \begin{Bmatrix} \sigma_x \\ \sigma_y \\ \sigma_{yz} \\ \sigma_{xz} \\ \sigma_{xy} \end{Bmatrix} = \begin{bmatrix} Q_{11}^c & Q_{12}^c & 0 & 0 & 0 \\ Q_{12}^c & Q_{22}^c & 0 & 0 & 0 \\ 0 & 0 & Q_{44}^c & 0 & 0 \\ 0 & 0 & 0 & Q_{55}^c & 0 \\ 0 & 0 & 0 & 0 & Q_{66}^c \end{bmatrix} \begin{Bmatrix} \varepsilon_x \\ \varepsilon_y \\ \gamma_{yz} \\ \gamma_{xz} \\ \gamma_{xy} \end{Bmatrix} \tag{13}$$

where:
for steel

$$Q_{11}^s = \frac{E^s}{1-v^2}, Q_{22}^s = Q_{11}^s, Q_{12}^s = \frac{vE^s}{1-v^2}$$
$$Q_{44}^s = Q_{55}^s = Q_{66}^s = G^s \ = \frac{E^s}{2(1+v)} \tag{14}$$

for concrete

$$Q_{11}^s = \frac{E^s}{1-v^2}, Q_{22}^s = Q_{11}^s, Q_{12}^s = \frac{vE^s}{1-v^2}$$
$$Q_{44}^s = Q_{55}^s = Q_{66}^s = G^s \ = \frac{E^s}{2(1+v)} \tag{15}$$

Using the NURBS basis functions, the displacement field $\boldsymbol{U}$ of the plate is approximated as

$$U(\xi,\eta) = \sum_{P=1}^{m\times n} R_P(\xi,\eta) U_P \tag{16}$$

where $\boldsymbol{U_P}$ is the vector of nodal degrees of freedom associated with the control point P

$$U_P = \begin{Bmatrix} u_{0P} \\ v_{0P} \\ w_{0P}^b \\ w_{0P}^s \end{Bmatrix} \tag{17}$$

Substituting Eq. (17) into Eq. (10) , the in-plane and shear strains can be rewritten as

$$U_P = \begin{Bmatrix} u_{0P} \\ v_{0P} \\ w_{0P}^b \\ w_{0P}^s \end{Bmatrix} \tag{18}$$

$$[\boldsymbol{\varepsilon}_0^T \quad \boldsymbol{\kappa}_b^T \quad \boldsymbol{\kappa}_s^T \quad \boldsymbol{\varepsilon}_s^T]^T = \sum_{P=1}^{m\times n}\left[[B_P^0]^T \quad \left[B_P^{bb}\right]^T \quad \left[B_P^{bs}\right]^T \quad [B_P^s]^T\right]^T \{U_P\} \tag{19}$$

Where

$$[B_P^0] = \begin{bmatrix} R_{P,x} & 0 & 0 \\ 0 & R_{P,y} & 0 \\ R_{P,y} & R_{P,x} & 0 \end{bmatrix} \tag{20}$$

$$\left[B_P^{bb} [] \begin{bmatrix} 0 & 0 & R_{P,xx} \\ 0 & 0 & R_{P,yy} \\ 0 & 0 & 2R_{P,xy} \end{bmatrix} \right] \tag{21}$$

$$\left[B_P^{bs}\right] = -\begin{bmatrix} 0 & 0 & R_{P,xx} \\ 0 & 0 & R_{P,yy} \\ 0 & 0 & 2R_{P,xy} \end{bmatrix} \tag{22}$$

$$[B_P^s] = \begin{bmatrix} 0 & 0 & R_{P,x} \\ 0 & 0 & R_{P,y} [] \end{bmatrix} \tag{23}$$

Using the variational principle for bending UHPC slabs, the weak form can be written as follows

$$\delta \int_\Omega \{\varepsilon\}^T \left[D^b\right]\{\varepsilon\} d\Omega + \delta \int_\Omega \{\gamma\}^T [A^s]\{\gamma\} d\Omega = \delta \int_\Omega q\{w\} d\Omega \tag{24}$$

where the stiffness matrices $\boldsymbol{A^s}, \boldsymbol{D^b}$ are given as follows

$$\left[D^b\right] = \begin{bmatrix} A_{11} & A_{12} & 0 & B_{11} & B_{12} & 0 & B_{11}^s & B_{12}^s & 0 \\ A_{12} & A_{22} & 0 & B_{12} & B_{22} & 0 & B_{12}^s & B_{22}^s & 0 \\ 0 & 0 & A_{66} & 0 & 0 & B_{66} & 0 & 0 & B_{66}^s \\ B_{11} & B_{12} & 0 & D_{11} & D_{12} & 0 & D_{11}^s & D_{12}^s & 0 \\ B_{12} & B_{22} & 0 & D_{12} & D_{22} & 0 & D_{12}^s & D_{22}^s & 0 \\ 0 & 0 & B_{66} & 0 & 0 & D_{66} & 0 & 0 & D_{66}^s \\ B_{11}^s & B_{12}^s & 0 & D_{11}^s & D_{12}^s & 0 & H_{11}^s & H_{12}^s & 0 \\ B_{12}^s & B_{22}^s & 0 & D_{12}^s & D_{22}^s & 0 & H_{12}^s & H_{22}^s & 0 \\ 0 & 0 & B_{66}^s & 0 & 0 & D_{66}^s & 0 & 0 & H_{66}^s \end{bmatrix} \tag{25}$$

$$[A^s] = \begin{bmatrix} A_{44}^s & 0 \\ 0 & A_{55}^s \end{bmatrix} \tag{26}$$

where A_{ij}, B_{ij}, etc., are the plate stiffness, defined by

$$\{A_{ij}, B_{ij}, D_{ij}\} = \int_{-\frac{h}{2}}^{hs-\frac{h}{2}} \{1, z, z^2\} Q_{ij}^s dz + \int_{hs-\frac{h}{2}}^{\frac{h}{2}} \{1, z, z^2\} Q_{ij}^c dz,, \ (i = 1,2,6)$$

$$B_{ij}^s = \int_{-\frac{h}{2}}^{hs-\frac{h}{2}} \psi\, Q_{ij}^s dz + \int_{hs-\frac{h}{2}}^{\frac{h}{2}} \psi\, Q_{ij}^c dz, \ (i = 1,2,6)$$

$$D_{ij}^s = \int_{-\frac{h}{2}}^{hs-\frac{h}{2}} z\, \psi Q_{ij}^s dz + \int_{hs-\frac{h}{2}}^{\frac{h}{2}} z\, \psi Q_{ij}^c dz, \ (i = 1,2,6)$$

$$H_{ij}^s = \int_{-\frac{h}{2}}^{hs-\frac{h}{2}} \psi^2\, Q_{ij}^s dz + \int_{hs-\frac{h}{2}}^{\frac{h}{2}} \psi^2\, Q_{ij}^c dz, \ (i = 1,2,6)$$

$$A_{ij}^s = \int_{-h/2}^{hs-h/2} \chi\, Q_{ij}^s dz + \int_{hs-h/2}^{h/2} \chi\, Q_{ij}^c dz, \ (i = 4,5) \tag{27}$$

The governing equation for static bending UHPC slabs in the following form

$$[K]\{U\} = \{F\} \tag{28}$$

where $[\boldsymbol{K}], \{\boldsymbol{U}\}$ and $\{\boldsymbol{F}\}$ denote stiffness matrix, generalized displacement, and force vector, respectively.

The global stiffness matrix *K* is given by

$$[K] = \int_{\Omega} \left\{ \{[B^0] \quad [B^{bb}] \quad [B^{bs}]\} [D^b] \begin{Bmatrix} [B^0] \\ [B^{bb}] \\ [B^{bs}] \end{Bmatrix} + [B^s]^T [A^s][B^s] \right\} d\Omega \tag{29}$$

and the load vector is given by

$$\{F\} = \int_{\Omega} q\{R\} d\Omega \tag{30}$$

where

$$\{R\} = \begin{Bmatrix} 0 \\ 0 \\ R_P \\ R_P \end{Bmatrix} \tag{31}$$

5. Numerical examples

5.1 Examples 1: Validation example

In this section, an numerical example is performed to verify the calculation results from the current study using the Isogeometric analysis method and compare with the analytical method. A

Table 1 Comparison of deflection in the center of slabs

h (cm)	h_s (cm)	Present-IGA	Analytics [40]			
			CPT	Error (%)	RPT	Error (%)
10	1.2	52.15	52.00	*0.27*	52.40	*0.49*
15	1.2	17.04	16.77	*1.60*	17.06	*0.10*
20	1.6	7.27	7.07	*2.71*	7.29	*0.30*
25	1.6	3.98	3.81	*4.28*	3.99	*0.29*
30	1.6	2.44	2.30	*6.03*	2.45	*0.36*
35	1.6	1.62	1.50	*7.98*	1.63	*0.50*

simply supported rectangular UHPC with dimensions a=3 m, b=3 m, modulus of elasticity and Poisson's ratio UHPC Ec=40 GPa (Ouyang *et al.* 2020), μ=0.25 and steel Es=20 0 GPa, μ_s=0.3 and the uniformly distributed load 10^6 N/m^2.

To investigate the steel UHPC composite slab by the isogeometric analysis with a thickness ranging from 10 to 35 cm and a steel layer thickness from 12 mm to 16 mm.

To validate the present approach, the the steel UHPC composite slab is solved using the Navier method (Reddy 2004) based on the classical (CPT) plate theory and refined plate theory (RPT). The results prediced using the analytical method are the close-form solution. The displacement calculation results using analytical method and isogeometric analysis methods are presented in Table 1.

The results shown in Table 1 clearly indicate that as the thickness of the slab increases, The error reaches approximately 8% when the plate thickness is 35 cm., the error in the slab's displacement compared to the result calculated using classical plate theory increases significantly. This can be explained by the fact that classical plate theory does not account for shear deformation, leading to smaller displacement values compared to calculations that consider shear deformations. The results in Table 1 also clearly show that the calculations using the isogeometric method have a very small error compared to the exact solution obtained through the analytical method using refined plate theory, the maximum error is only up to 0.5%.

5.2 Examples 2

In this example, the rectangular steel UHPC composite slab with simply supported and clamped boundary conditions are investigated, with the dimensions and material properties as follows: a=3 m, b=4 m, modulus of elasticity and Poisson's ratio UHPC Ec=40 GPa, μ=0.25 and steel Es=200 GPa, μs=0.3 and the uniformly distributed load 10^6 N/m^2.

The results of the steel UHPC composite slab displacements shown in Fig .2 indicate a significant reduction in displacement under the clamped boundary condition.

Table 2 shows the deflection at the center of the slabs for various thicknesses of the plate and different thicknesses of material layers.

Fig. 3 shows the displacements in the central slabs with thicknesses ranging from 15 to 35 cm, steel plate thicknesses ranging from 10 to 20 mm and two boundary conditions: simply supported slab in Fig. 3(a), clapped supported slab in Fig. 3(b). Fig. 3 clearly shows a sharp decrease in transverse displacement as thickness increases. In the case the thickness of the plate remains constant and the increasing thickness of the steel UHPC slabs, the transverse displacement does

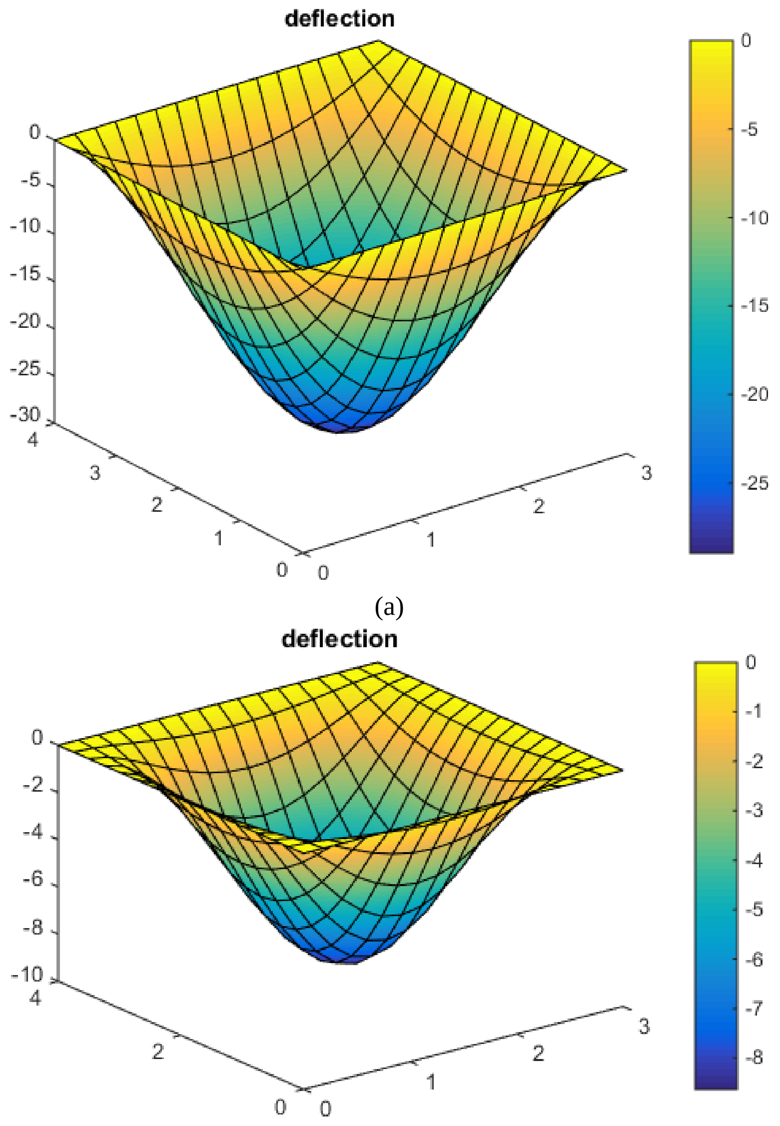

(b)

Fig. 2 Displacement of slabs with h=15 cm, h_s=10 mm; (a) simply support slab, (b) clapped slab

Table 2 The table of displacement at the center of the steel UHPC composite slab

h (cm)	Simply Support Plates h_s (mm)			Clapped Plates h_s (mm)		
	10 mm	16 mm	20 mm	*hs* 10 mm	*hs* 16 mm	*hs* 20 mm
15	28,96	25,97	24,84	8,63	7,71	7,34
20	13,19	11,80	11,21	4,01	3,58	3,39
25	7,17	6,44	6,11	2,22	2,00	1,89
30	4,36	3,94	3,74	1,39	1,25	1,19
35	2,87	2,61	2,48	0,93	0,85	0,81

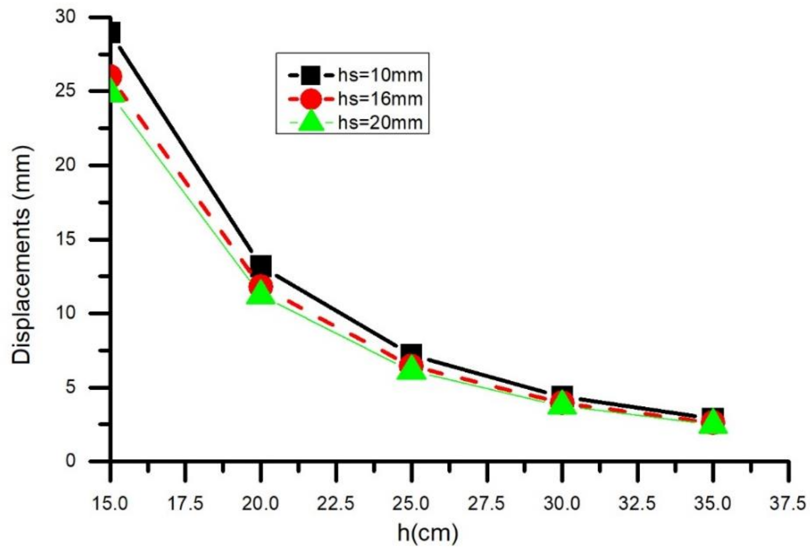

(a) Simply supported slab

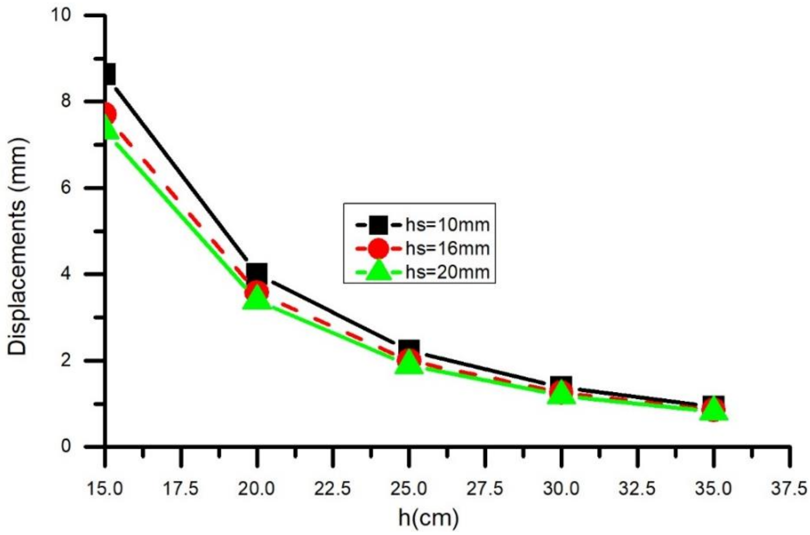

(b) Clapped slab

Fig. 3 Deflection at central plates; (a) simply supported slab, (b) clapped supported slab

not decrease much. In fact, when the thickness of the steel plate increases, the plate’s stiffness will also increase slightly, causing the displacement to decrease by a small amount.

6. Conclusions

The paper used refined plate theory to build stress-strain relationships of steel UHPC composite slabs, then combined the NUBRS function to build equations for the isogeometric analysis method. The MATLAB program has been successfully developed based on established steel

UHPC composite slab formulas.

Performing comparative examples with the analytical method shows the high accuracy of the method developed in this study. Due to the effect of shear deformation as the thickness of the slab increases, the displacement of the plate is larger than the result when calculated by classical theory to 8% as the surveyed data. Numerical examples have shown a clear influence of the thickness of the slab's material layers on the displacement. Based on the consideration of higher-order shear deformations, the numerical example's results predicted by the present approach are good agreement with the exact solution obtained using the analytical method based on the refined plate theory. When the thickness of the slab or steel layer increases, the displacement of the simply and the clamped slab is significantly reduced.

Steel UHPC composite slabs have higher strength and rigidity than reinforced concrete slabs, it is possible to reduce the height of the plate while still ensuring the strength and service limit state.

Acknowledgments

This research is funded by Ministry of Education and Training (MoET), Vietnam under the grand number B2023-GHA-08.

References

Abokifa, M. and Moustafa, M.A. (2021), "Experimental behavior of precast bridge deck systems with non-proprietary UHPC transverse field joints", *Mater.*, **14**(22), 6964. https://doi.org/10.3390/ma14226964.

Cottrell, J.A., Hughes, T.J. and Bazilevs, Y. (2009). *Isogeometric Analysis: Toward Integration of CAD and FEA*, John Wiley & Sons.

Cuong, N.H. and Quang, N.D. (2020), "Experimental study on flexural behavior of prestressed and non-prestressed textile reinforced concrete plates", *Transp. Commun. Sci. J.*, **71**(1), 37-45. https://doi.org/10.25073/tcsj.71.1.5.

El-Helou, R.G. and Graybeal, B.A. (2022), "Shear behavior of ultrahigh-performance concrete pretensioned bridge girders", *J. Struct. Eng.*, **148**(4), 04022017. https://doi.org/10.1061/(ASCE)ST.1943-541X.0003279.

Ghalehnovi, M., Yousefi, M., Karimipour, A., de Brito, J. and Norooziyan, M. (2020), "Investigation of the behaviour of steel-concrete-steel sandwich slabs with bi-directional corrugated-strip connectors", *Appl. Sci.*, **10**, 8647. http://doi.org/10.3390/app10238647.

Gunes, O., Yesilmen, S., Gunes, B. and Ulm, F.J. (2012), "Use of UHPC in bridge structures: Material modeling and design", *Adv. Mater. Sci. Eng.*, **2012**, 319285. http://doi.org/10.1155/2012/319285.

Haruna, S., Adamu, M., Ibrahim, Y., Aliyu, M.M. and Haruna, S. (2023), "Internal curing of ultra-high-performance concrete: A comprehensive overview", *J. Mech. Behav. Mater.*, **32**(1), 20220282. http://doi.org/10.1515/jmbm-2022-0282.

Hien, T.D. and Noh, H.C. (2017), "Stochastic isogeometric analysis of free vibration of functionally graded plates considering material randomness", *Comput. Meth. Appl. Mech. Eng.*, **318**, 845-863. https://doi.org/10.1016/j.cma.2017.02.007.

Hien, T.D., Khoa, N.T., Tien, D.N., Hang, D.T., Tung, N.X. and Diem, N.D. (2022), "Approximation solution for steel concrete beam accounting high-order shear deformation using trigonometric-series", *J. Mater. Eng. Struct.*, **9**, 599-605.

Hughes, T.J.R., Cottrell, J.A. and Bazilevs, Y. (2005), "Isogeometric analysis: CAD, finite elements, NURBS, exact geometry and mesh refinement", *Comput. Meth. Appl. Mech. Eng.*, **194**, 4135-4195.

https://doi.org/10.1016/j.cma.2004.10.008.

Ibrahim, M., Farhat, M., Issa, M. and Hasse, J. (2017), "Effect of material constituents on mechanical and fracture mechanics properties of ultra-high-performance concrete", *ACI Mater. J.*, **114**, 453-465. http://doi.org/10.14359/51689717.

Jun, X., Yuan, S. and Chen, W. (2019), "Isogeometric analysis of gradient-enhanced damaged plasticity model for concrete", *Comput. Concrete*, **23**, 171-188. http://doi.org/10.12989/cac.2019.23.3.171.

Kodsy, A. and Morcous, G. (2022), "Shear strength of Ultra-High-Performance Concrete (UHPC) beams without transverse reinforcement: Prediction models and test data", *Mater.*, **15**, 4794. https://doi.org/10.3390/ma15144794.

Le-Manh, T., Luu-Anh, T. and Lee, J. (2016), "Isogeometric analysis for flexural behavior of composite plates considering large deformation with small rotations", *Mech. Adv. Mater. Struct.*, **23**, 328-336. http://doi.org/10.1080/15376494.2014.981616.

Liao, Q., Xie, X. and Jiangtao, Y. (2022), "Numerical investigation on dynamic performance of reinforced ultra-high ductile concrete-ultra-high performance concrete panel under explosion", *Struct. Concrete*, **23**(6), 3601-3615. http://doi.org/10.1002/suco.202100919.

Luu, X.B. and Kim, S.K. (2023), "Finite element modeling of interface behavior between normal concrete and ultra-high performance fiber-reinforced concrete", *Build.*, **13**(4), 950. https://doi.org/10.3390/buildings13040950.

Micelli, F., Renni, A., Kandalaft, A.G. and Moro, S. (2020). "Fiber-reinforced concrete and ultrahigh-performance fiber-reinforced concrete materials", *New Materials in Civil Engineering*, Butterworth-Heinemann.

Nguyen, D.L., Le, H.V., Vu, T.B.N., Nguyen, V.T. and Tran, N.T. (2023), "Evaluating fracture characteristics of ultra-high-performance fiber-reinforced concrete in flexure and tension with size impact", *Constr. Build. Mater.*, **382**, 131224, https://doi.org/10.1016/j.conbuildmat.2023.131224.

Nhiem, T.D. (2020), "Report on solutions, design and construction techniques to strengthen Thang Long bridge deck", *Proceedings of the Technological Solutions to Repair and Strengthen Thang Long Bridge Deck*, University of Transport and Communications, Ha Noi.

Olajumoke, A. and Dundu, M. (2019), "Dynamic performance of steel plate-strengthened reinforced concrete slabs in bending", *Advances in Engineering Materials, Structures and Systems: Innovations, Mechanics and Applications*, CRC Press.

Ouyang, X., Shi, C., Wu, Z., Li, K., Shan, B. and Shi, J. (2020), "Experimental investigation and prediction of elastic modulus of ultra-high performance concrete (UHPC) based on its composition", *Cement Concrete Res.*, **138**, 106241. https://doi.org/10.1016/j.cemconres.2020.106241.

Pham, Q.H., Tran, T.T. and Nguyen, P.C. (2023), "Dynamic response of functionally graded porous-core sandwich plates subjected to blast load using ES-MITC3 element", *Compos. Struct.*, **309**, 116722. https://doi.org/10.1016/j.compstruct.2023.116722.

Phuc, P.M. (2020), "Using phase field and third-order shear deformation theory to study the effect of cracks on free vibration of rectangular plates with varying thickness", *Transp. Commun. Sci. J.*, **71**, 853-867. https://doi.org/10.47869/tcsj.71.7.10.

Piegl, L.A. and Tiller, W. (1997), *The NURBS Book*, Springer, Berlin, New York.

Pu, B., Wang, X., Li, W. and Feng, J. (2022), "Analytical model formulation of steel plate reinforced concrete walls against hard projectile impact", *Appl. Sci.*, **12**(1), 518. https://doi.org/10.3390/app12010518.

Reddy, J.N. (2003), *Mechanics of Laminated Composite Plates and Shells: Theory and Analysis*, CRC Press.

Shimpi, R.P. and Patel, H.G. (2006), "A two variable refined plate theory for orthotropic plate analysis", *Int. J. Solid. Struct.*, **43**, 6783-6799. http://doi.org/10.1016/j.ijsolstr.2006.02.007.

Shuwen, D., Shao, X., Yan, B., Wang, Y. and Li, H. (2020), "on flexural performance of girder-to-girder wet joint for lightweight steel-UHPC composite bridge", *Appl. Sci.*, **10**, 1335. https://doi.org/10.3390/app10041335.

Ta, H.D. and Nguyen, P.C. (2020), "Perturbation based stochastic isogeometric analysis for bending of functionally graded plates with the randomness of elastic modulus", *Lat. Am. J. Solid. Struct.*, **17**,

https://doi.org/10.1590/1679-78256066.
Ta, H.D. and Noh, H.C. (2015), "Analytical solution for the dynamic response of functionally graded rectangular plates resting on elastic foundation using a refined plate theory", *Appl. Math. Model.*, **39**, 6243-6257. https://doi.org/10.1016/j.apm.2015.01.062.
Thang, P.B. and Anh, L.V. (2021), "Structural analysis of steel-concrete composite beam bridges utilizing the shear connection model", *Transp. Commun. Sci. J.*, **72**, 811-823. https://doi.org/10.47869/tcsj.72.7.4.
Tien, D.N., Tung, N.X. and Lam, N.N. (2024), "Analytical solution for bending steel concrete composite plates considering the shear deformation effect", *Eng. Technol. Appl. Sci. Res.*, **14**(5), 16090-16094. https://doi.org/10.48084/etasr.7801.
Tran, L.V., Ferreira, A.J.M. and Nguyen-Xuan, H. (2013), "Isogeometric analysis of functionally graded plates using higher-order shear deformation theory", *Compos. Part B: Eng.*, **51**, 368-383. http://doi.org/10.1016/j.compositesb.2013.02.045.
Wu, C., Li, J. and Su, Y. (2018), "Ultra-high performance concrete columns", *Development of Ultra-High Performance Concrete against Blasts: From Materials to Structures*, Woodhead Publishing, 215-282.
Wu, C., Li, J. and Su, Y. (2018), *Development of Ultra-High Performance Concrete Against Blasts: from Materials to Structures*, Woodhead Publishing.
Xiao, R., Song, C., Bin, S., Guo, R. and Chen, H. (2022), "Design and experimental study of a replaceable steel-UHPC composite bridge deck", *Struct.*, **40**, 1107-1120. https://doi.org/10.1016/j.istruc.2022.04.091.
Ye, Y.Y., Smith, S.T., Zeng, J.J., Zhuge, Y. and Quach, W.M. (2021), "Novel ultra-high-performance concrete composite plates reinforced with FRP grid: Development and mechanical behaviour", *Compos. Struct.*, **269**, 114033. https://doi.org/10.1016/j.compstruct.2021.114033.
Zhang, Q., Nguyen-Thanh, N., Li, W., Zhang, A.M., Li, S. and Zhou, K. (2023), "A coupling approach of the isogeometric-meshfree method and peridynamics for static and dynamic crack propagation", *Comput. Meth. Appl. Mech. Eng.*, **410**, 115904. https://doi.org/10.1016/j.cma.2023.115904.
Zhu, J., Ding, J. and Wang, Y. (2022), "Numerical and theoretical studies on shear behavior of steel-UHPC composite beams with waffle slab", *J. Build. Eng.*, **47**, 103913. https://doi.org/10.1016/j.jobe.2021.103913.